We are IntechOpen, the world's leading publisher of Open Access books

Built by scientists, for scientists

6,900
Open access books available

185,000
International authors and editors

200M
Downloads

Our authors are among the

154
Countries delivered to

TOP 1%
most cited scientists

12.2%
Contributors from top 500 universities

CLARIVATE ANALYTICS
BOOK CITATION INDEX
INDEXED

WEB OF SCIENCE™

Selection of our books indexed in the Book Citation Index
in Web of Science™ Core Collection (BKCI)

Interested in publishing with us?
Contact book.department@intechopen.com

Numbers displayed above are based on latest data collected.
For more information visit www.intechopen.com

Electrical Manipulation of a Single Nanowire by Dielectrophoresis

Marcos Vinicius Puydinger dos Santos, Fanny Béron,
Kleber Roberto Pirota, José Alexandre Diniz and
Stanislav Moshkalev

Additional information is available at the end of the chapter

Abstract

Nanowires (NWs), due to their unique highly anisotropic characteristics, hold a great promise to be used in wide technological fields, such as building blocks for data storage and memory, advanced scanning probes, and biotechnological applications. In addition, given the high sensitivity to their environment, NWs can be used as sensor for a number of applications. The fabrication and electrical characterization of NW-based devices can be achieved after proper placing of NWs between electrodes, which represents one of the major challenges in this field. The dielectrophoresis (DEP) method can be used to trap electrically neutral NWs by the application of an alternating electric field between a pair of electrodes. Here, we present a systematic study of DEP parameters as well as electrodes geometry for NW deposition. This method presents a suitable protocol for deposition in a useful and coherent fashion of post-growth electrodeposited NWs and further electrical characterization. This can be used for investigation of the fundamental transport properties of individual NWs and fabrication of NW-based devices, such as sensors and field-effect transistors.

Keywords: nanowire, dielectrophoresis, electrically-induced manipulation, electrical characterization

1. Introduction

Nanowires (NWs) represent adequate elements for electronic devices that require ultra-low power consumption, given their low current levels and high sensitivity they usually exhibit [1–5]. Their one-dimensional geometry, as well as unique possibilities for engineering of

magnetic, electric and optic properties, make them to be promising nanostructures for a variety of applications, including chemical and biological sensors [6, 7], field-effect transistors [8], advanced scanning probes and magnetic sensors [9], light-emitting diodes [10], lasers [11] and photodetectors [12, 13]. Furthermore, NWs can be synthesized through a number of techniques, such as metal-organic epitaxy [14], focused-ion-beam (FIB) [8], focused-electron-beam-induced deposition (FEBID) [15], electron beam lithography [5] and electrodeposition [16, 17], yielding to unique attributes, such as particular crystallographic properties, geometry and axial/coaxial heterostructures [18].

However, despite significant advances that have been made in NWs synthesis and devices characterization, post-growth manipulation and placement of single NWs in a coherent and useful fashion remains one of the major challenges to fabricate and study the electrical transport properties of NW-based devices [19–21], especially the ones made of a single NW. So far, numerous techniques have been proposed to realize NW-based devices from already existing NWs assembly, such as atomic force microscopy nanomanipulation [22], Langmuir-Blodgett films [23], fluidic-directed assembly [24], dry-transfer printing [25], although with relatively low NW yield for precise positioning of functional system [18].

Alternatively, NWs suspended in a dielectric electrolytic solution can be manipulated through electric fields [1, 5, 26–31]. When an electrically neutral NW is subjected to a non-uniform electric field, the electric charges redistribution within the NW as well as in the solid-liquid interface builds up an electric dipole moment [32]. Thus, as the Coulomb forces on either sides of the dipole can differ in direction and intensity, a net force is exerted on the NW, which is known as the dielectrophoretic force [19, 27–32]. The force direction depends on the relative polarizabilities of the electrolyte and of the NW, inducing the latter move towards or against the region of higher electric field intensity. Such motion of nanoparticles is termed as dielectrophoresis (DEP) [19, 20, 26–32]. DEP has a tremendous advantage over the aforementioned techniques, as it relies on the possibility of working with NWs of a wide range of conductivities as well as arbitrary substrates including those that require low-temperature processing such as flexible substrates [18]. Since DEP directly depends on the dielectric properties of the particles and diluting medium, as well as the nanoparticles geometry, it allows high process selectivity [18, 32]. Moreover, large electrode arrays can be properly defined by lithography such that DEP can take place concomitantly in a large number of electrodes, leading to high throughput.

However, to fully realize these capabilities, DEP must be carefully controlled to ensure that wires are precisely placed at desired locations. Therefore, it is necessary to determine the relevant parameters that affect DEP experiment and how to control them. In this work, nickel nanowires (NiNWs) with length of around 4 μm and 35 nm of diameter, obtained by electrodeposition into pores of anodized alumina membrane and further dispersed in a dimethyl-formamide (DMF) electrolytic solution, were manipulated by DEP in order to make electrical contact between a pair of electrodes. Electrodes geometry and DEP electrical parameters were varied to evaluate the NiNW deposition efficiency by this technique. The materials for NW and diluting medium presented in this work were arbitrarily chosen to provide a proof-of-concept for the reader, though a selection of several NW materials and diluting medium is provided as well. In addition, COMSOL simulation supports experimental results on NWs deposition.

2. Dielectrophoresis

2.1. DEP theory

The electric force induced by non-uniform electric fields on polarizable and anisotropic nanoparticles can be used to properly align and trap individual liquid-suspended nanoparticles at predefined locations of a substrate. This force, termed as the DEP force, uses AC electric fields to selectively move neutral nanoparticles (e.g. NiNWs) dispersed in a dielectric diluting medium (e.g. DMF) (**Figure 1a**) [26, 32]. It relies on the polarizability differences between the NW and the DMF. The electrodes shape yields to a non-uniform electric field, which is proportional to the applied voltage. It creates a net force on the NW that exceeds the viscous force between the NW and the fluid, inducing a preferential NW movement towards the electrodes gap (**Figure 1b**). Although the discussion presented in this work considers only NW as example of particles, the analysis also applies to other anisotropic particles such as nanotubes, nanorods or sheets.
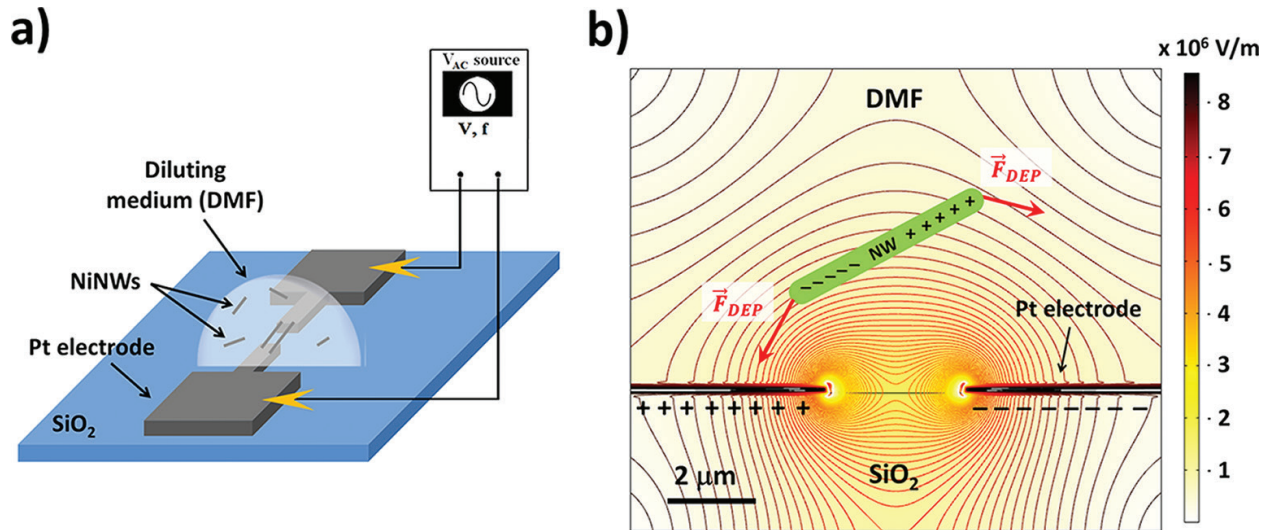

Figure 1. (a) Schematic of the DEP experiment. Adapted with permission from [33]. Copyright 2015 by American Vacuum Society. (b) DEP mechanism, in which the electric-field gradient induces attraction forces on the nanowire towards the gap between electrodes.

This force can be expressed by [5, 30, 33]

$$F_{DEP} = \frac{1}{8} \pi \varphi^2 L \varepsilon_{DMF} Re\{K\} \nabla \left| E \right|^2 \tag{1}$$

where φ and L represent, respectively, the NW diameter and length, $Re\{\}$ is the real term and $K(\omega)$ the Clausius-Mossoti factor—or the so-called complex polarization factor—expressed as function of electrical permittivities of NiNW and DMF (respectively, ε_{NiNW} and $\varepsilon_{DMF} = 36.7\,\varepsilon_0$, where ε_0 is the electrical permittivity of vacuum) [5]:

$$K(\omega) = \frac{\varepsilon^*_{NiNW}(\omega) - \varepsilon^*_{DMF}(\omega)}{\varepsilon^*_{NiNW}(\omega) + 2\,\varepsilon^*_{DMF}(\omega)}. \tag{2}$$

The imaginary component of the complex permittivity, ε^*, depends on the conductivity, σ, and the applied field angular frequency, ω:

$$\varepsilon^*(\omega) = \varepsilon - j\frac{\sigma}{\omega}. \tag{3}$$

Thus, the real-term frequency-dependent factor of the DEP force is given by

$$Re\{K\} = \frac{\omega^2(\varepsilon_{DMF}\varepsilon_{NiNW} - \varepsilon_{DMF}^2) + (\sigma_{DMF}\sigma_{NiNW} - \sigma_{DMF}^2)}{\varepsilon_{DMF}^2\omega^2 + \sigma_{DMF}^2}. \tag{4}$$

The complex polarization factor's dependence on the permittivity introduces a relationship between the dielectrophoretic force and the frequency of the applied field. Eqs. (5) and (6) present the high- and low-frequency limits, respectively:

$$\omega \to \infty : Re\{K\} = \frac{\varepsilon_{NiNW} - \varepsilon_{DMF}}{\varepsilon_{DMF}} \tag{5}$$

$$\omega \to 0 : Re\{K\} = \frac{\sigma_{NiNW} - \sigma_{DMF}}{\sigma_{DMF}}. \tag{6}$$

At the high-frequency limit, the DEP force is determined by the relative permittivity of the NW and the DMF, while at low frequencies the force will be a function of their relative conductivities. Within this frequency range, the transition between those two regimes is evidenced by plotting the DEP force against frequency. Inserting the appropriate NW and diluting liquid electrical conductivities (respectively, σ_{NiNW} = 1.4 × 10^7 Ω^{-1} m^{-1} and σ_{DMF} = 2.5 × 10^{-4} Ω^{-1} m^{-1}) in Eq. (4), one may calculate the frequency-dependence of F_{DEP}, where a reduction of DEP force is observed for frequencies higher than 100 kHz (**Figure 2a**).

At 500 kHz and 1 MHz, the force approximately decreases by one and two orders of magnitude, respectively. However, this model does not consider fluid dynamics effects, such as
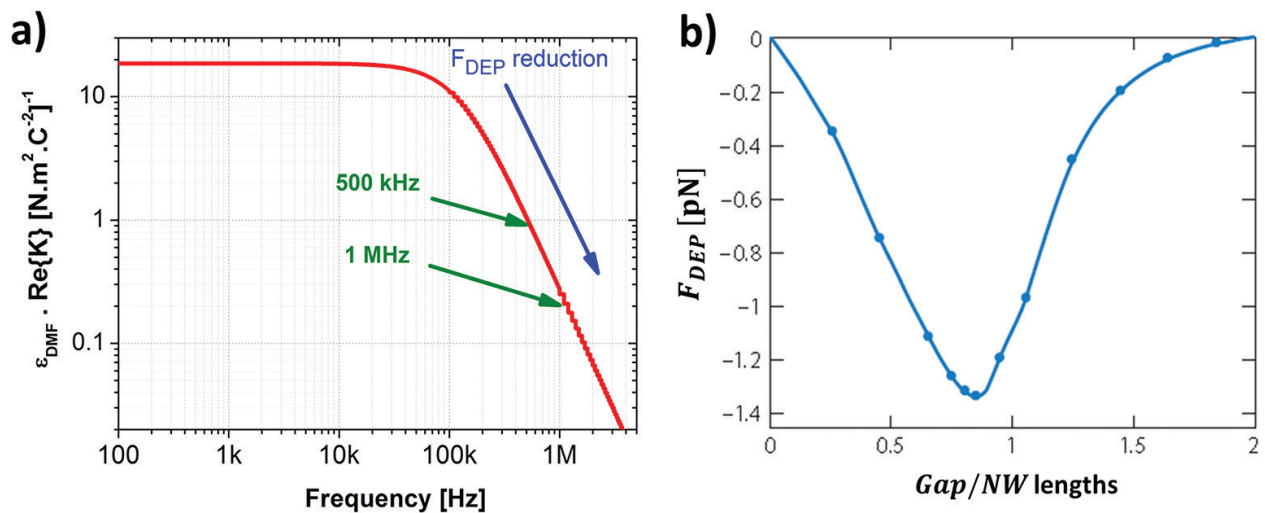

Figure 2. (a) Real part of the complex polarization factor (proportional to F_{DEP}), as function of frequency, for NiNW diluted in DMF medium, showing force reduction for frequencies above 100 kHz. Adapted with permission from [33]. Copyright 2015 by American Vacuum Society. (b) DEP force as function of the ratio between electrodes gap length and NW length, showing that the attraction force is maximized in the minimum of the force curve. Adapted with permission from [35]. Copyright 2012 by American Chemical Society.

AC electroosmosis [20]. For the electrostatics parameters of NiNW and DMF, this effect can reduce the force for frequencies above 1–10 kHz [19], as will be discussed in the next section. Other effects also act on the NW, such as viscous and frictional forces, fluid flow and NW-surface interactions [5, 34]. Therefore, the DEP force needs to overcome those effects in order to effectively perform deposition. Additionally, the DEP force will always depend on the ratio between the electrodes gap and NW lengths (**Figure 2b**), as this ratio influences the electric field lines density covering the NW and thus the applied torque [35]. The DEP force is maximized (attraction force, see in **Figure 2b**) for a ratio of around 0.8, since the electric field gradient and strength effects are the largest for this ratio [36]. For a smaller gap, the DEP force decreases because, despite that the electric field applied at the gap centre remains constant, it is reduced around the entire NW length. On the other hand, for a larger gap, the DEP force also decreases, simply because the electric field around the NW is less intense [5, 35, 36]. In this work, for NiNWs length of (4 ± 1) µm, we used a gap length of (2.5 ± 0.3) µm, yielding a ratio of (0.6 ± 0.2), which is near the maximum DEP force condition.

Furthermore, Eq. (1) exhibits a quadratic dependence of DEP force with the applied voltage, which increases the amount of deposited NWs in the gap region [5, 33]. In this work, we fixed the peak-to-peak voltage (V_{PP}) to 3 V, since it produces a reasonable DEP force without overheating and consequently damaging the NiNWs during DEP process.

Finally, although we have presented DEP analysis for NiNWs dissolved in a DMF solution, one might be interested in experiments involving NWs composed of different materials. Thus, we present **Table 1**, which provides an overview of reported parameters from the literature that optimizes DEP force.

Nanowire material	Medium	Potential (V)	Frequency (kHz)	Electrode gap (µm)	Electric field (V µm^{-1})
Au	Methanol	0.97	150	2	0.485
Au	Methanol	10	>100	2	5
Au-biotin	Methanol	0.18	1000	2	0.09
ZnO	Ethanol	5	1000	6–10	0.833–0.5
ZnO	Ethanol	5	1000	4	1.25
Ag	Ethanol	0.1	5	4	0.025
Ag or Au	H$_2$O or EtOH	0.2	100	30	0.00667
Rh rods	Acetone	10	Unknown	5–30	2–0.333
CNT[a]	Acetone	45	Unknown	5–30	9–1.5
p-Si	Benzyl alcohol	110	10	40	2.75
Si	IPA[b] and H$_2$O	0.35	0.5	2	0.175

[a]CNT, carbon nanotube.
[b]IPA, isopropanol.

Table 1. Overview of optimized parameters reported in literature for DEP alignment of different types of NW (adapted from [19]).

2.2. AC electroosmosis

Under the influence of an AC electric field, electrolytes on planar microelectrodes exhibit fluid flow tangential to the electrode surface. The Coulomb force generated from this electric field on the solution interfacial charges (**Figure 3a**) leads to fluid flow along the electrode surface away from the gap in a process termed AC electroosmosis [20, 37]. This effect is triggered by applying an alternating potential difference of the order of kHz at low voltages (around 1 V) to each pair of electrodes. It has been exploited in microfluidics to pump fluids in microcapillaries where surface forces preclude traditional pumping by pressure differentials.
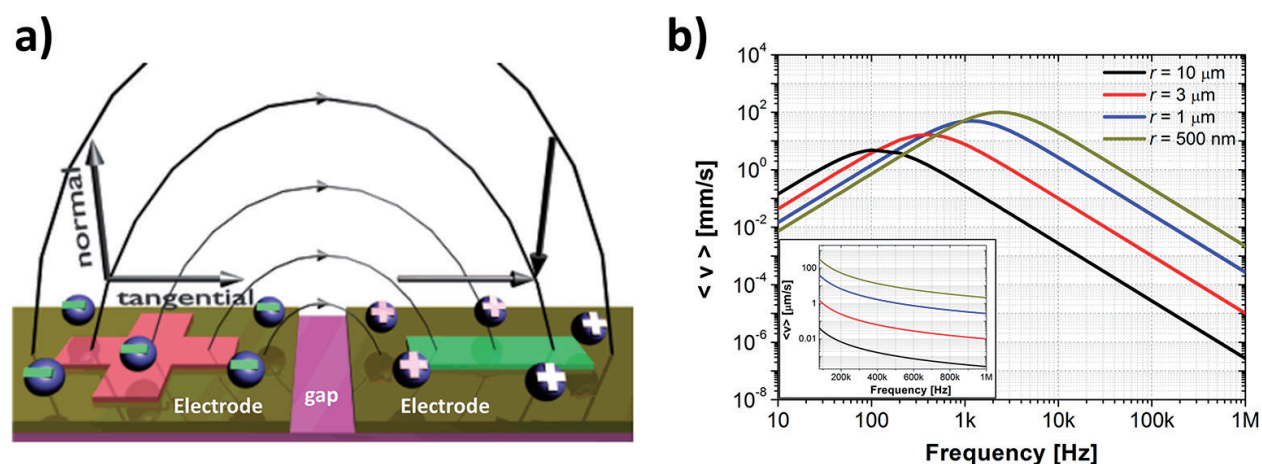

Figure 3. (a) Surface-bound interfacial charges (spheres), induced by electrodes, interact with the tangential component of electric field (curved lines), thus moving the fluid along the electrode surface away from the electrode gap. Field lines originating from the positively charged electrode and ending on the negatively charged one represent the force experienced by positive charge (negative charge experiences force in opposite direction). This force leads to fluid flow along the electrodes away from the gap. Adapted with permission from [20]. Copyright 2007 by American Chemical Society. (b) Average velocity of the fluid obtained for $V_0 = 3\ V_{PP}$ for several distances from the electrodes gap centre. *Inset*: Frequency working range utilized in this work, in which the average velocity decreases about two orders of magnitude between 100 kHz and 1 MHz for any distance, d.

The physical mechanism responsible for driving the flow relies on non-uniformities in the AC electric fields at the gap region. They produce an electric force on the surface-bound interfacial charges, yielding a non-zero time-averaged electroosmotic slip velocity at the electrodes surface [38]. The AC electroosmotic effect can produce fluid velocities from hundreds of μm/s up to a few mm/s in some cases [20, 37]. It should be noted that this fluid flow is distinct from the one originated from electro-thermal effects, which are found at higher frequencies and higher electrolyte conductivities [38].

For symmetrical, coplanar microelectrode gaps such as those reported in this work, AC electroosmosis produces fluid flow along the electrode surface directed away from the centre of the electrode gap. The average fluid velocity near the electrode surface is given by [20, 37, 38]

$$\langle v \rangle = \frac{1}{8} \frac{\varepsilon_{DMF} V_0^2 \Omega^2}{\eta d (1 + \Omega^2)^2},$$ (7)

where d is the position along the electrodes surface with its origin at the gap centre, V_0 is the applied voltage between electrodes, $\eta = 0.92$ mPa s the electrolyte viscosity and the dimensionless frequency Ω is given by

$$\Omega = \omega d \frac{\varepsilon_{DMF}}{\sigma_{DMF}} \frac{\pi}{2} \kappa,$$ (8)

where $\kappa = (15 \text{ nm})^{-1}$ is the reciprocal of electrolyte Debye length for induced double charge on the electrodes. Eq. (7) gives a bell-shaped profile for the frequency dependence of the velocity. The average velocity is small at both low and high frequencies. In the former case, most of the electric field relies in the interfacial charged layer between the electrode and the electrolyte, preventing the tangential field to extend very far into the solution. In the latter, the interfacial charged layer is thin because the charged species in the electrolyte are not fast enough to follow the rapidly changing polarities of the electrodes. On the contrary, at intermediate frequencies, the velocity can be considerably large [37]. **Figure 3b** shows average velocities of DMF for $d = 500$ nm, 1 µm, 3 µm and 10 µm from the electrodes gap centre, at 3 V. For these DEP conditions, the fluid velocity at the gap region will range from a few nanometres to tens of millimetres per second, depending on the frequency, which produces additional forces on the NWs and thus considerably influences NWs deposition.

3. Efficiency evaluation of DEP: a case study

In the next sections, DEP efficiency was evaluated for NiNW trapping on Pt electrodes, chosen due to the low-oxidation rate and relatively low-electrical resistivity that allows further two-wire electrical transport measurements on a single isolated NW. The DEP parameters, such as voltage and frequency, were varied in order to optimize the number of NWs that make contact between the electrodes, for which statistical evaluation was performed. The total electric field distribution over the gap area was simulated using COMSOL Multiphysics simulation tool to support experimental results.

3.1. Electrodes fabrication

Pt electrodes were defined on a SiO_2/Si structure. First, a 300 nm-thick SiO_2 layer was grown on an n$^+$-type Si (1 0 0) wafer (electrical resistivity of 1–10 Ω cm) by wet thermal oxidation in a conventional furnace, in order to act as a dielectric layer (**Figure 4a**). Then, photolithography was performed to define the electrodes region. An 80 nm-thick Pt layer was sputtered by a physical vapour deposition system, and lift-off process was carried out to define electrodes (**Figure 4b**). Three different electrode geometries were fabricated to evaluate the effect of electrode shape on DEP force, further denominated 1 (rectangular extremities), 2 (circular extremities) and 3 (narrow extremities) (**Figure 5**).
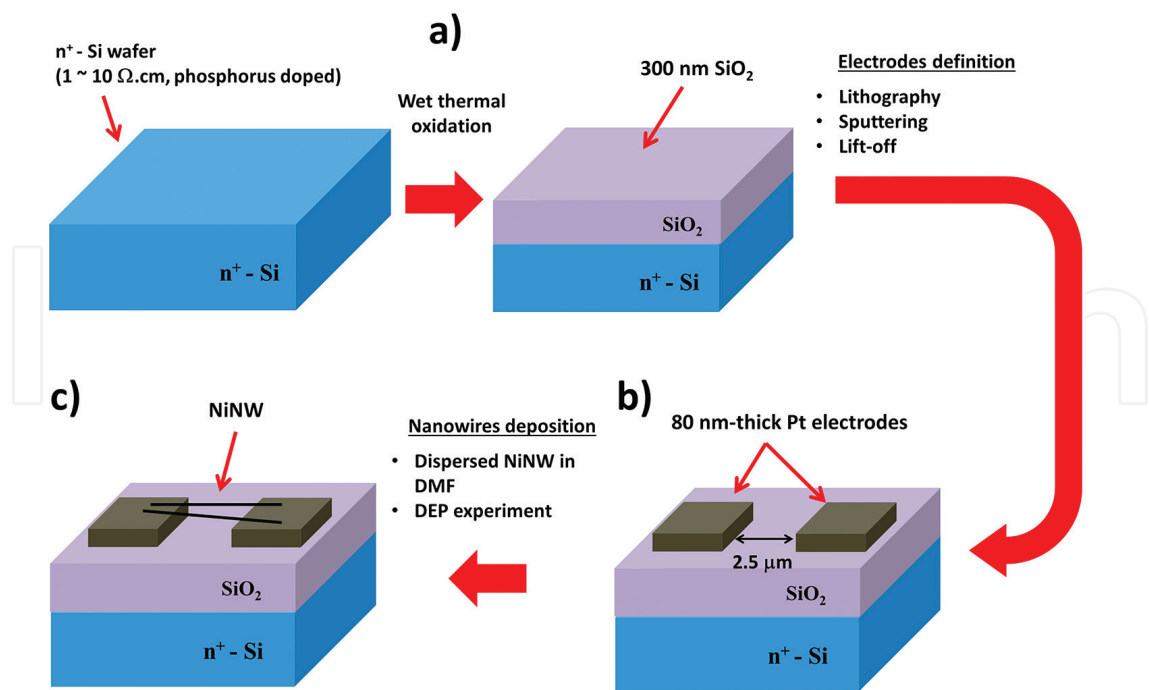
Figure 4. Schematics of experimental procedures: (a) dielectric layer formation on top of n⁺-Si wafer by thermal oxidation; (b) electrodes definition by photolithography and lift-off; (c) NiNW deposition on electrodes by DEP experiment. Adapted with permission from [33]. Copyright 2015 by American Vacuum Society.
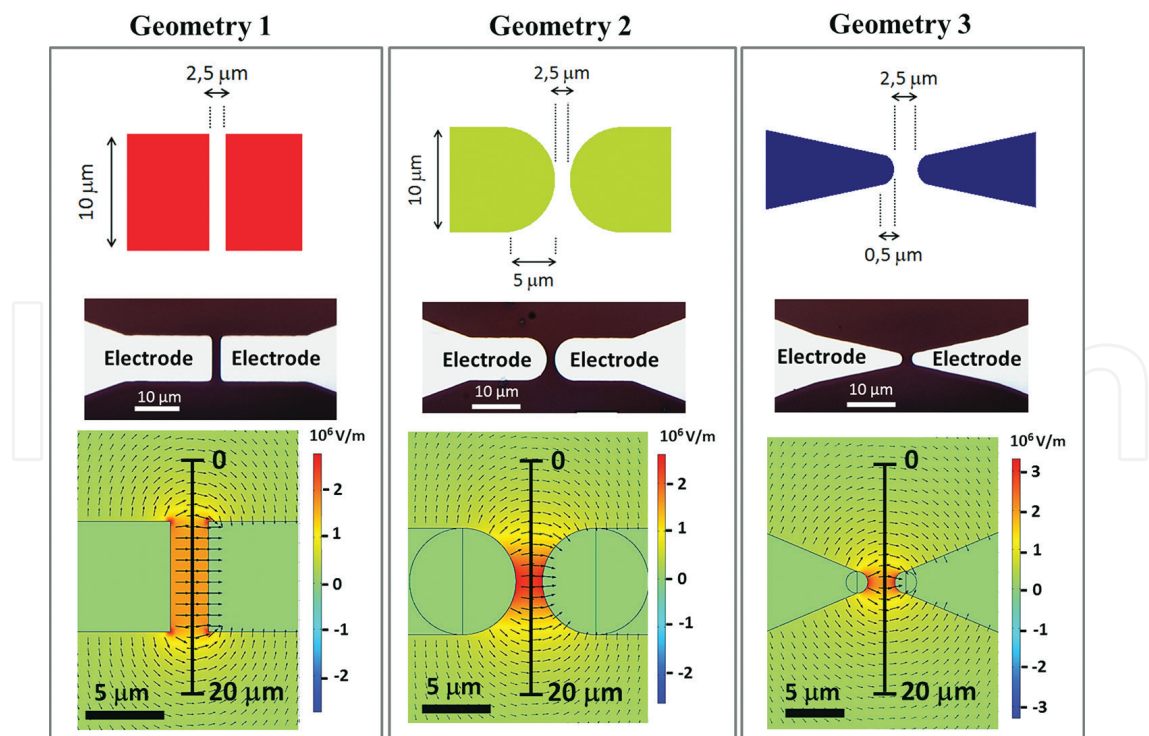

Figure 5. Schematics (top), optical microscopy (centre) and total electric field simulations, using COMSOL Multiphysics tool (below) of the three geometries tested for the Pt electrodes. The 20 μm line was taken for evaluation of the electric field profile for each geometry, as presented in **Figure 8**. Reprinted with permission from [33]. Copyright 2015 by American Vacuum Society.

3.2. NiNWs fabrication and DEP experimental procedure

NiNWs of 4 ± 1 μm-long and 35 ± 5 nm of diameter were fabricated via pulsed electrodeposition into anodized alumina membrane [16, 17]. A 1 M NaOH chemical etching solution at 24°C under agitation was employed to release the NWs from the porous alumina membrane. They were then cleaned with isopropanol and rinsed with deionized water in order to remove organic remains and further dispersed in DMF to avoid NWs clusters formation. The NiNW deposition was performed by DEP (**Figure 4c**), conducted with a HP 8116A pulse/function generator configured with 3 V_{PP} and null offset. The sinusoidal signal was generated for a frequency range between 50 kHz and 1 MHz. Before DEP process, the solution (concentration of ca. 10^8 NiNW mL^{-1}) was sonicated for 120 s at room temperature, in order to uniformly disperse the NiNWs in the DMF. Then, 1 μL solution volume was placed in the gap region and the DEP parameters were applied on each pair of electrodes during 60 s. The DMF excess was immediately rinsed with deionized water and dried with N$_2$. For each set of DEP parameters, the experiment was repeated ca. 100 times to ensure statistical reliability.

Visual inspection of the gap region by scanning electron microscopy (SEM) was used to evaluate the DEP efficiency for the three electrode geometries and the frequency range used (**Figure 6**). An experiment in which at least one NiNW was deposited—and made electrical contact with a pair of electrodes—was considered as success. For each geometry and frequency, we normalized the number of successes by the total number of experiments. Thus, it was possible to evaluate the efficiency percentage of NiNW deposition (**Figure 7a**) and the average number of deposited NiNW for the successful cases (**Figure 7b**), as a function of the DEP frequency and electrode geometry.
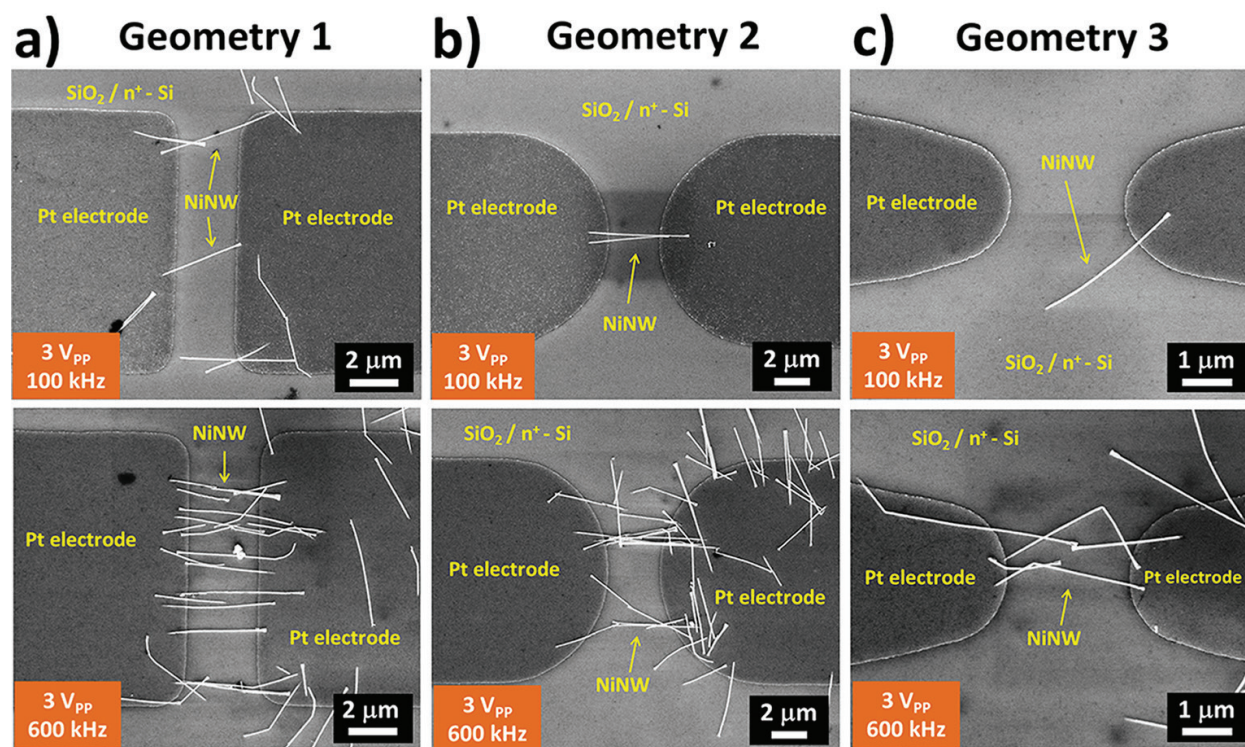

Figure 6. SEM analysis of NiNWs deposited on Pt electrodes for (a) geometry #1, (b) geometry #2 and (c) geometry #3, after DEP experiment (V_{PP} = 3 V, frequency = 100 kHz (upper row) and 600 kHz (lower row)). Reprinted with permission from [33]. Copyright 2015 by American Vacuum Society.
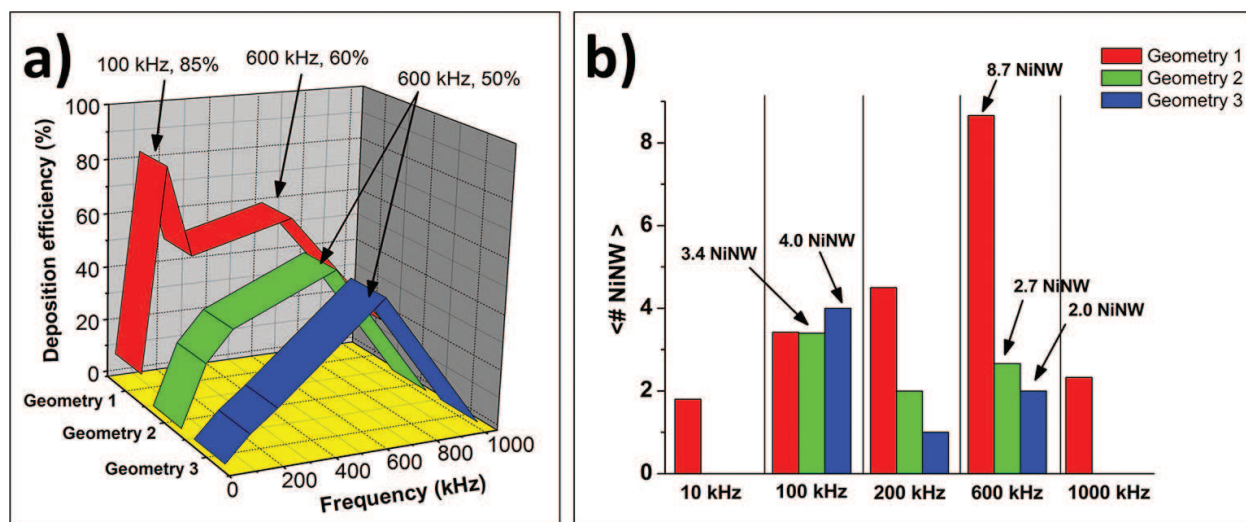
Figure 7. Charts of (a) deposition efficiency and (b) average number of deposited NiNW, obtained for DEP experiment as a function of electric field frequency, for the three electrodes geometries. Reprinted with permission from [33]. Copyright 2015 by American Vacuum Society.

First, it should be noted that DEP and AC electroosmosis might be considered as competing mechanisms for NWs deposition between electrodes. While DEP force is the main mechanism for NW trapping, AC electroosmosis, which occurs simultaneously to DEP, can induce fluid turbulence in the electrodes gap region, thus reducing the probability of success as well as the number of trapped NiNWs. Therefore, as expected from both Eq. (4) and fluid dynamics effects predictions, the DEP efficiency at 10 kHz and 1MHz was almost null, obtaining success only for geometry 1 (8% and 16%, respectively). For frequencies close to 10 kHz, the average AC electroosmosis velocity near the gap is relatively high (**Figure 3b**) and this turbulence prevents the DEP force to trap the NiNW towards the electrodes. On the other hand, for frequencies close to 1 MHz, the DEP force is about two orders of magnitude lower than the one in the range of kHz (**Figure 2a**).

Furthermore, the maximum efficiency obtained for geometry 1 was 85% at 100 kHz, while an efficiency of 60% was reached at 600 kHz. On the other hand, the DEP process was less efficient for geometries 2 and 3, both with the maximum value of 50% obtained for 600 kHz. This discrepancy may be assigned to electric field homogeneity over the electrodes gap, which is larger for geometry 1 than for geometries 2 and 3. The electrode areas are smaller in geometry 2 and 3 cases, which could create inhomogeneities and thus reduce the trapping effect in the gap region. Moreover, the maximum efficiency obtained for geometries 2 and 3 at 600 kHz still represents the frequency region that simultaneously maximizes the DEP force and minimizes the electroosmosis effect. On the other hand, for geometry 1, the larger electrode area increases the probability of success and more NiNWs are captured during DEP process. **Figure 8** presents the simulated total electric field intensity along a 20 μm transversal cross-section in the gap region, indicated in **Figure 5**. We assume that the product between the peak height, h, and its full-width half-maximum, σ, is related to the deposition efficiency. The decreasing product value for geometry 1 to 3 is in agreement with the obtained efficiency results.
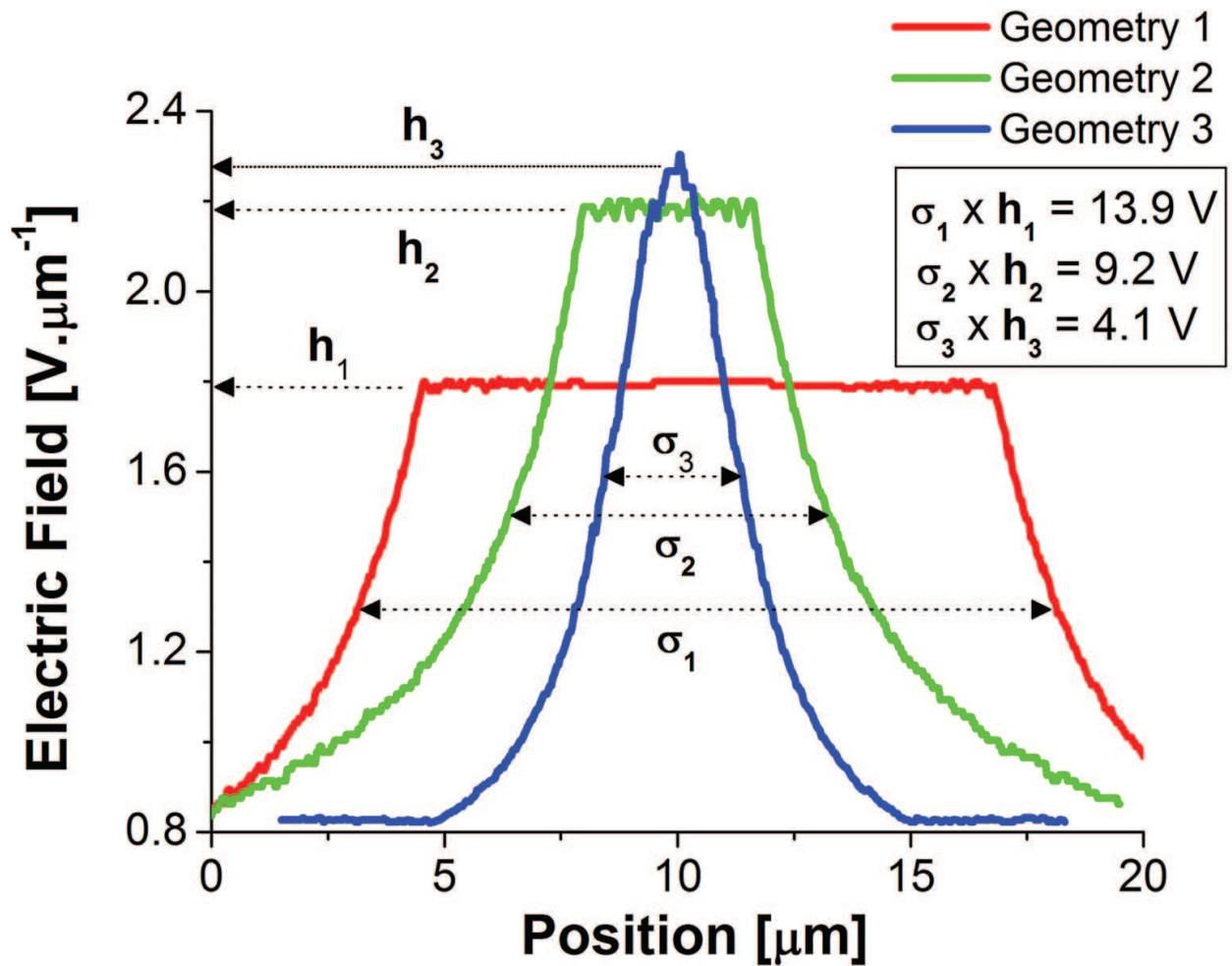
Figure 8. Total simulated electric field amplitude profile for the 20 μm transversal line shown in **Figure 4** for the three geometries, indicating the trapping efficiency to be related to the product between the peak height and its full-width half-maximum. Reprinted with permission from [33]. Copyright 2015 by American Vacuum Society.

Typically, several NiNWs were simultaneously deposited during the successful experiments, with an average number ranging from 1.0 to 8.7. Interestingly, for each investigated geometry, the maximum number of deposited NiNWs was not reached for the frequency yielding the highest efficiency. For geometry 1, only 3.4 NiNWs were deposited at 100 kHz (85% of efficiency), while a peak of 8.7 ones was attained at 600 kHz (60% of efficiency) (**Figure 7**). This result may also be attributed to the crossover between DEP and AC electroosmosis mechanisms. While the DEP force is expected to be maximized at around 100 kHz, the average fluid velocity near the gap is estimated to be close to the maximum peak value (about hundreds of micrometres/s), which limits the number of NiNWs making contact. On the contrary, at a frequency of 600 kHz, the average electroosmosis velocity reduces almost two orders of magnitude—compared to 100 kHz—yielding to less turbulence in the gap region and, therefore, a larger number of NiNWs making electrical contact between electrodes.

The situation is similar for geometries 2 and 3, but inverting the frequencies for which the efficiency and number of deposited NiNWs were maximized. The larger number of deposited NiNWs even for lower efficiency frequency may be attributed to the distortion of the electric field

in the electrodes gap created by the first deposited NiNW, reducing the DEP force on the remaining NiNWs dispersed in the DMF solution and thus reducing the number of NiNWs present at higher frequencies. As shown in **Figure 9**, the electric field intensity in the gap region decreases abruptly when the first NiNW makes contact between electrodes, as the electric charges present in the metallic electrodes mainly flows through the NW. However, geometry 1 still presents a larger area, which favours more NiNWs to be present at 600 kHz, as aforementioned.
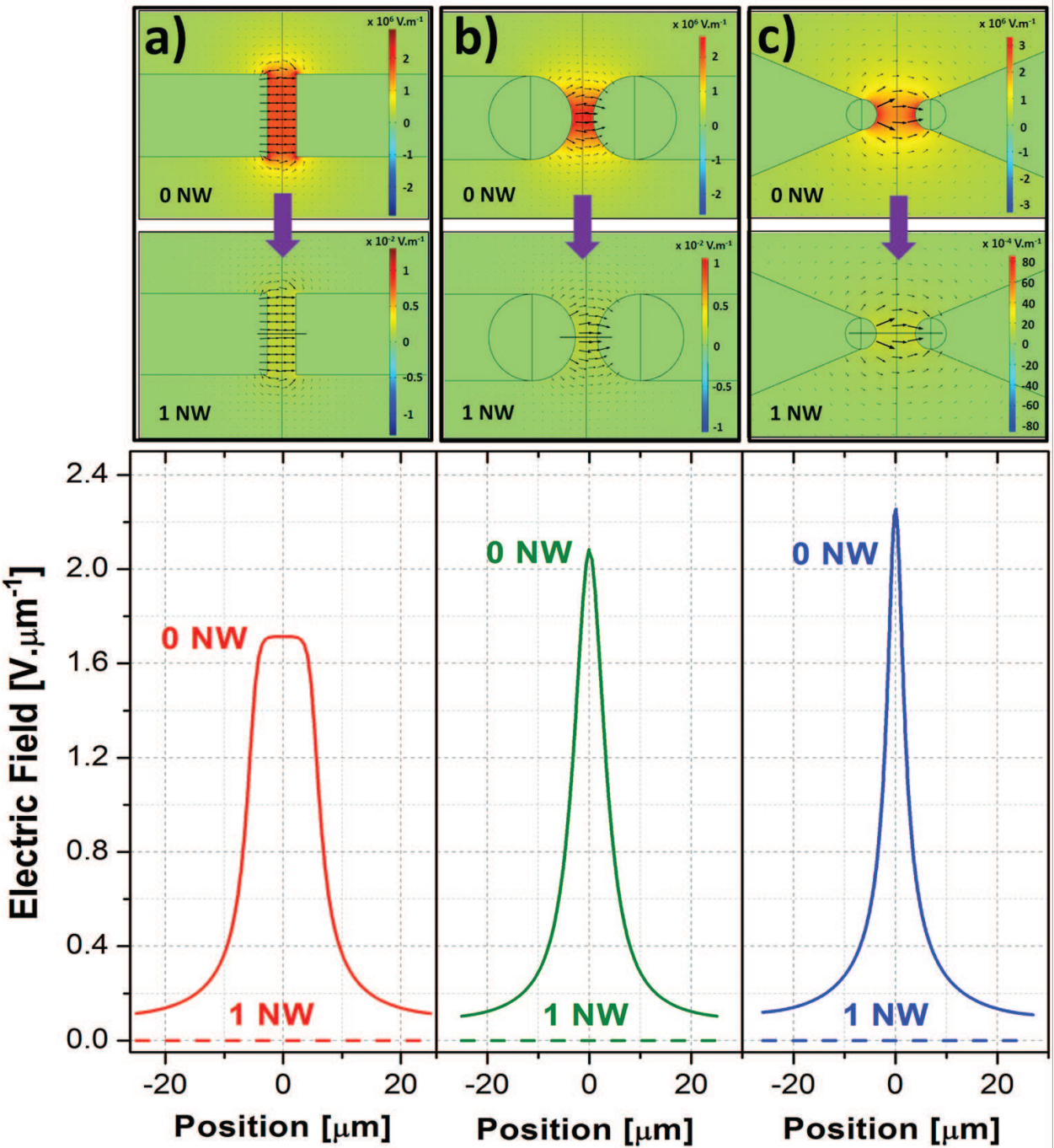

Figure 9. Total electric field simulation (using COMSOL Multiphysics) (top) and curves representing a 50 μm-long cross-section transversal line to the electrodes pair in the gap centre (bottom) for (a) geometry 1, (b) geometry 2 and (c) geometry 3. For all geometries, the total electric field substantially decreases when the first NW makes contact, reducing the probability for the second NW to make contact as well.

Globally, geometry 1 is the most efficient for DEP of NiNWs, as one can obtain efficiency up to 85% (for 3 V_{PP} and 100 kHz). However, our aim, when using DEP process, is to evaluate the transport properties of a single NiNW or only a few of them. Thus, a reasonable result is obtained when only a few NiNWs are present between electrodes. Therefore, geometries 2 and 3 reach ideal average values of NiNW (2.7 and 2.0, respectively, for 600 kHz), still with 50% of efficiency.

3.3. Electrical characterization of a single NiNW isolated by DEP

In order to evaluate the adequacy of DEP protocol for building single NW-based devices or studying fundamental properties of isolated NWs, electrical current-voltage (I-V) measurements were obtained with a Keithley 2400 source meter by applying current (without exceeding 1 nW of power to avoid damaging NiNWs due to heat dissipation) while measuring voltage with a two-wire setup. Parallel equivalent resistance as a function of the number of deposited NWs was measured and presented in a logarithm scale (**Figure 10a**). The linear fit slope of $-1.0 \pm 0.1\ \Omega\ \mathrm{NiNW^{-1}}$ is in good agreement with the ideal case ($-1\ \Omega\ \mathrm{NiNW^{-1}}$) indicating that all the NWs made proper electrical contact after DEP process. This was accomplished due to metal-like behaviour of both the electrode and the NW. It is worth to mention that the NiNW resistance is about two orders of magnitude larger than the electrodes and cables resistance as well as the contact resistance between the metallic NW and electrodes, making it possible to use a two-wire set-up for this electrical characterization. However, for processes that require DEP of semiconductor and oxide-based NWs as well as carbon-based nanostructures, post-annealing processes are usually required to make proper electrical contact and thus reduce the contact resistance [39, 40]. Alternatively, one may perform DEP of NW using four electrodes in a 4-probes measurement setup for contact resistance subtraction.

In addition, the electric resistivity of one single NiNW, ρ, was measured as a function of temperature, T, using a Physical Property Measurement System (PPMS), in the range of 2–300 K (**Figure 10b**), showing metallic behaviour, as expected. The residual resistivity value of a single NiNW is $\rho_0 = 27\ \mu\Omega$ cm, which is in good agreement with the ones with similar dimensions found in literature [17, 33].
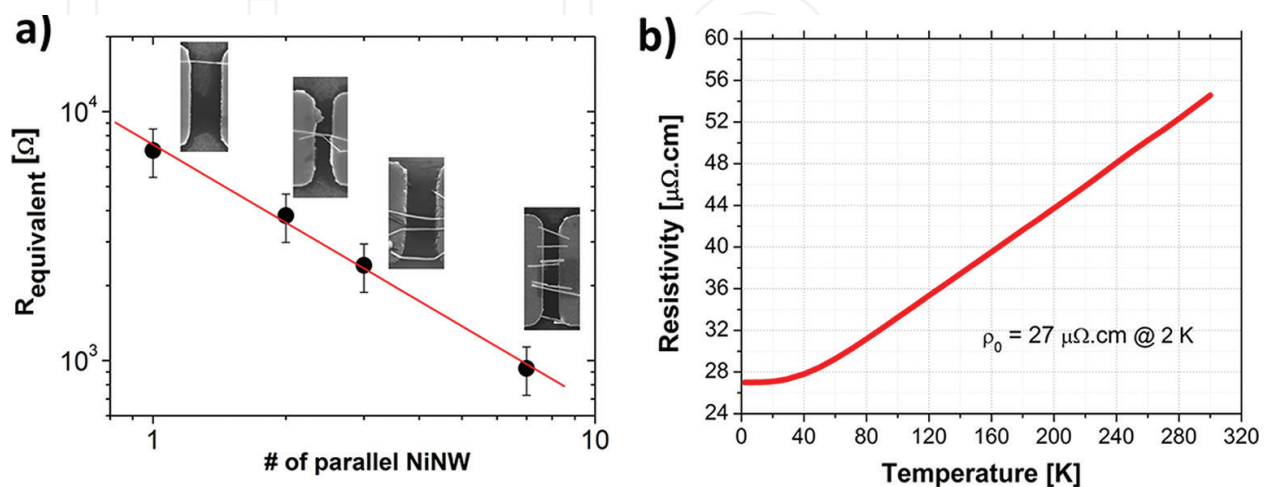

Figure 10. (a) Equivalent parallel resistance versus number of parallel-deposited NiNWs and (b) ρ x T curve of one single NiNW, showing metallic behaviour and a residual resistance of 27 $\mu\Omega$ cm at 2 K. Adapted with permission from [16]. Copyright 2013 by Brazilian Microelectronics Society.

4. Conclusion

This work presented DEP trapping of NiNWs between Pt electrodes defined by photo-lithography and lift-off. It consists of a powerful protocol for building unique and useful devices. The deposition efficiency and average number of NiNWs were evaluated as a function of the electrodes geometry and DEP frequency. Moreover, the influence of AC electroosmotic fluid flow (as a cross-over mechanism with DEP) could be observed in the mismatch between the frequencies for the largest NiNWs deposition efficiency and the largest number of deposited NiNWs. The maximum deposition efficiencies for square electrodes were 85 and 60% for 100 and 600 kHz, respectively, for averages of 3.4 and 8.7 deposited NiNWs. On the other hand, the efficiency was maximized at 600 kHz for the circular and narrow geometries, with value of 50% and averages of 2.7 and 2.0 NiNWs, respectively. This behaviour can be attributed to electric field inhomogeneities and lower trapping area over the gap present between electrodes in these geometries. For the square electrodes, since it presents a larger electrode area, it captures more NiNWs during DEP process and increases the probability of success, even with electric field intensity slightly lower than circular and narrow geometries. Adequate individual isolated NiNW electrical characterization was allowed by the successful DEP experiment of metallic NWs on the top of metallic electrodes. Additionally, post-annealing processes may be required for improving contact resistance of semiconductor and metal-oxide NWs as well as carbon-based nanostructures to metallic electrodes.

Finally, the DEP process seems to be a promising feature to evaluate fundamental properties of individual NWs as well as to build NW-based sensor devices, since they can be manipulated and isolated with relatively high efficiency. Thus, their individual electrical, thermal and/or optical output signals (in response to the environment stimulus) can be further processed. In addition, NiNWs present ferromagnetic properties, which allow their low current levels to be controlled through magnetic fields. Thus, they can be thought as an alternative for single-NW magnetic sensors as well as a promising alternative to the traditional Si-based MOSFET devices.

Author details

Marcos Vinicius Puydinger dos Santos[1,2,3]*, Fanny Béron[1], Kleber Roberto Pirota[1], José Alexandre Diniz[2] and Stanislav Moshkalev[3]

*Address all correspondence to: puyding@ifi.unicamp.br

1 Institute of Physics Gleb Wataghin, University of Campinas, Campinas-SP, Brazil

2 Faculty of Electrical Engineering and Computing, University of Campinas, Campinas-SP, Brazil

3 Center for Semiconductor Components and Nanotechnology, University of Campinas, Campinas-SP, Brazil

References

[1]   Wu J, Yin B, Wu F, Myung Y, Banerjee P. Charge transport in single CuO nanowires. Applied Physics Letters. 2014;**105**(18):183506-1-183506-5. DOI: 10.1063/1.4900966

[2]   Li M, Li WH, Zhang J, Alici G, Wen W. A review of microfabrication techniques and dielectrophoretic microdevices for particle manipulation and separation. Journal of Physics D: Applied Physics. 2014;**47**(6):63001-1-63001-29. DOI: 10.1088/0022-3727/47/6/063001

[3]   Seo K-WW, Lee J-HH, Cho NG, Kang SJ, Kim H-KK, Na S-II, Koo H-WW, Kim T-WW. Simple brush painted Ag nanowire network on graphene sheets for flexible organic solar cells. Journal of Vacuum Science and Technology A. 2014;**32**(6):61201-1-61201-6. DOI: 10.1088/0022-3727/47/6/063001

[4]   Ou MN, Yang TJ, Harutyunyan SR, Chen YY, Chen CD, Lai SJ. Electrical and thermal transport in single nickel nanowire. Applied Physics Letters. 2008;**92**(6):063101-1–063101-3. DOI: 10.1063/1.2839572

[5]   Boote JJ, Evans . Dielectrophoretic manipulation and electrical characterization of gold nanowires. Nanotechnology. 2005;**16**(9):1500-1505. DOI: 10.1088/0957-4484/16/9/015.

[6]   Huang J, Wan Q. Gas sensors based on semiconducting metal oxide one-dimensional nanostructures. Sensors. 2009;**9**:9903-9924. DOI: 10.3390/s91209903

[7]   Cui Y, Wei Q, Park H, Lieber . Nanowire nanosensors for highly sensitive and selective detection of biological and chemical species. Science. 2001;**293**:1289-1292. DOI: 10.1126/science.1062711.

[8]   Puydinger dos Santos MV, Lima LPB, Diniz JA, Godoy Filho J. Fabrication of p-type silicon nanowires for 3D FETs using focused ion beam. Journal of Vacuum Science and Technology B. 2013;**31**(6):06FA01-1-06FA01-6. DOI: 10.1116/1.4823763

[9]   De Teresa JM, Fernández-Pacheco A. Present and future applications of magnetic nanostructures grown by FEBID. Applied Physics A: Materials Science & Processing. 2014;**117**(4):1645-1658. DOI: 10.1007/s00339-014-8617-7

[10] Svensson CPT, Mårtensson T, Trägårdh J, Larsson C, Rask M, Hessman D, Samuelson L, Ohlsson J. Monolithic GaAs/InGaP nanowire light emitting diodes on silicon. Nanotechnology. 2008;**19**:305201-1-305201-6. DOI: 10.1088/0957-4484/19/30/305201

[11] Zhou H, Wissinger M, Fallert J, Hauschild R, Stelzl F, Klingshirn C, Kalt H. Ordered, uniform-sized ZnO nanolaser arrays. Applied Physics Letters. 2007;**91**:181112-1-181112-3. DOI: 10.1063/1.2805073

[12] Novotny CJ, Yu ET, Yu PKL. InP Nanowire/polymer hybrid photodiode. Nano Letters. 2008;**8**(3):775-779. DOI: 10.1063/1.2805073

[13] Soci C, Zhang A, Xiang B, Dayeh SA, Aplin DPR, Park J, Bao XY, Lo YH, Wang D. ZnO nanowire UV photodetectors with high internal gain. Nano Letters. 2007;**7**(4):1003-1009. DOI: 10.1021/nl070111x

[14] Yoshimura M, Tomioka K, Hiruma K, Hara S, Motohisa J, Fukui T. Growth and characterization of InGaAs nanowires formed on GaAs(111)B by selective-area metal organic vapor phase epitaxy. Japanese Journal of Applied Physics. 2010;**49**:04DH08-1-04DH08-5. DOI: 10.1143/JJAP.49.04DH08

[15] Puydinger dos Santos M V., Velo MF, Domingos RD, Zhang Y, Maeder X, Guerra-Nuñez C, Best JP, Béron F, Pirota KR, Moshkalev S, Diniz JA, Utke I. Annealing-based electrical tuning of cobalt–carbon deposits grown by focused-electron-beam-induced deposition. ACS Applied Materials and Interfaces. 2016;**8**:32496-32503. DOI: 10.1021/acsami.6b12192

[16] Puydinger dos Santos MV, Velo MF, Domingos RD, Bettini J, Diniz JA, Béron F, Pirota KR. Electrodeposited nickel nanowires for magnetic-field effect transistor (MagFET). Journal of Integrated Circuits and Systems. 2016;**11**(1):13-18.

[17] Leitao DC, Sousa CT, Ventura J, Amaral JS, Carpinteiro F, Pirota KR, Vazquez M, Sousa JB, Araujo JP. Characterization of electrodeposited Ni and Ni80Fe20 nanowires. Journal of Non-Crystalline Solids. 2008;**354**:5241-5243. DOI: 10.1016/j.jnoncrysol.2008.05.088

[18] Raychaudhuri S, Dayeh SA, Wang D, Yu ET. Precise semiconductor nanowire placement through dielectrophoresis. Nano Letters. 2009;**9**(6):2260-2266. DOI: 10.1021/nl900423g

[19] Maijenburg AW, Maas MG, Rodijk EJB, Ahmed W, Kooij ES, Carlen ET, Blank DHA, ten Elshof JE. Dielectrophoretic alignment of metal and metal oxide nanowires and nanotubes: A universal set of parameters for bridging prepatterned microelectrodes. Journal of Colloid and Interface Science. 2011;**335**(2):486-493. DOI: 10.1016/j.jcis.2010.12.011

[20] Gierhart BC, Howitt DG, Chen SJ, Smith RL, Collins SD. Frequency dependence of gold nanoparticle superassembly by dielectrophoresis. Langmuir. 2007;**23**(24):12450-12456. DOI: 10.1021/la701472y

[21] Vijayaraghavan A, Sciascia C, Dehm S, Lombardo A, Bonetti A, Ferrari AC, Krupke R. Dielectrophoretic assembly of high-density arrays of individual graphene devices for rapid screening. ACS Nano. 2009;**3**(7):1729-1734. DOI: 10.1021/nn900288d

[22] Decossas S, Mazen F, Baron T, Brémond G, Souifi A. Atomic force microscopy nanomanipulation of silicon nanocrystals for nanodevice fabrication. Nanotechnology. 2003;**14**:1272-1278. DOI: 10.1088/0957-4484/14/12/008

[23] Whang D, Jin S, Wu Y, Lieber CM. Large-scale hierarchical organization of nanowire arrays for integrated nanosystems. Nano Letters. 2003;**3**(9):1255-1259. DOI: 10.1021/nl0345062

[24] Huang Y, Xiangfeng D, Qingqiao W, Lieber C. Directed assembly of one-dimensional nanostructures into functional networks. Science. 2001;**291**:630-633. DOI: 10.1126/science.291.5504.630

[25] Javey A, Nam S, Friedman RS, Yan H, Lieber CM. Layer-by-layer assembly of nanowires for three-dimensional, multifunctional electronics. Nano Letters. 2007;**7**(3):773-777. DOI: 10.1021/nl063056l

[26] Pohl HA. The motion and precipitation of suspensoids in divergent electric fields. Journal of Applied Physics. 1951;**22**(7):869-871. DOI: 10.1063/1.1700065

[27] Xie C, Chen B, Ng CO, Zhou X, Wu J. Numerical study of interactive motion of dielectrophoretic particles. European Journal of Mechanics B/Fluids. 2015;**49**:208-216. DOI: 10.1016/j.euromechflu.2014.08.007

[28] Kang S. Dielectrophoretic motion of two particles with diverse sets of the electric conductivity under a uniform electric field. Computers & Fluids. 2014;**105**:231-243. DOI: 10.1016/j.compfluid.2014.09.029

[29] Schukfeh MI, Storm K, Hansen A, Thelander C, Hinze P, Beyer A, Weimann T, Samuelson L, Tornow M. Formation of nanogaps in InAs nanowires by selectively etching embedded InP segments. Nanotechnology. 2014;**25**:465306-1-465306-6. DOI: 10.1088/0957-4484/25/46/465306

[30] Hamdi FS, Français O, Dufour-Gergam E, Le Pioufle B. How medium osmolarity influences dielectrophoretically assisted on-chip electrofusion. Bioelectrochemistry. 2014;**100**:27-35. DOI: 10.1016/j.bioelechem.2014.05.004

[31] Freer EM, Grachev O, Stumbo DP, Duan X, Martin S, Stumbo DP. High-yield self-limiting single-nanowire assembly with dielectrophoresis. Nature Nanotechnology. 2010;**5**:525-530. DOI: 10.1038/nnano.2010.157

[32] Pohl HA. Dielectrophoresis: The Behavior of Neutral Matter in Non-Uniform Electric Fields. 1st ed. New York: Cambridge University Press; 1978. 579 p.

[33] Puydinger dos Santos M V., Lima LPB, Mayer RA, Béron F, Pirota KR, Diniz JA. Dielectrophoretic manipulation of individual nickel nanowires for electrical transport measurements. Journal of Vacuum Science and Technology B. 2015;**33**(3):031804-1-031804-8. DOI: 10.1116/1.4918732

[34] Dimaki M, Bøggild P. Dielectrophoresis of carbon nanotubes using microelectrodes: a numerical study. Nanotechnology. 2004;**15**:1095-1102. DOI: 10.1088/0957-4484/15/8/039

[35] Smith BD, Mayer TS, Keating CD. Deterministic assembly of functional nanostructures using nonuniform electric fields. Annual Review Physical Chemistry. 2012;**63**:241-263. DOI: 10.1146/annurev-physchem-032210-103346

[36] Liu Y, Chung JH, Liu WK, Ruoff RS. Dielectrophoretic assembly of nanowires. Journal of Physical Chemistry B. 2006;**110**(29):14098-14106. DOI: 10.1021/jp061367e

[37] Green NG, Ramos A, González A, Morgan H, Castellanos A. Fluid flow induced by non-uniform ac electric fields in electrolytes on microelectrodes. I. Experimental measurements. Physical Review E. 2000;**61**(4):4011-4018. DOI: 10.1103/PhysRevE.61.4019

[38] Ramos A, González A, Castellanos A, Green NG, Morgan H. Pumping of liquids with ac voltages applied to asymmetric pairs of microelectrodes. Physical Review E: Statistical Nonlinear Soft Matter Physics. 2003;**67**:056302-1-056302-11. DOI: 10.1103/PhysRevE.67.056302

[39] Rouxinol FP, Gelamo R V., Amici RG, Vaz AR, Moshkalev SA. Low contact resistivity and strain in suspended multilayer graphene. Applied Physics Letters. 2010;**97**:253104-1-253104-4. DOI: 10.1063/1.3528354

[40] Li M, Anderson W, Chokshi N, DeLeon RL, Tompa G. Laser annealing of laser assisted molecular beam deposited ZnO thin films with application to metal-semiconductor-metal photodetectors. Journal of Applied Physics. 2006;**100**:053106-1-053106-4. DOI: 10.1063/1.2344811